Pertanika J. Sci. & Technol. 28 (2): 493 - 508 (2020)

PERTANIKA JOURNALS

SCIENCE & TECHNOLOGY

Journal homepage: http://www.pertanika.upm.edu.my/

System Identification of Helical Strakes Suppressed Vortex-induced Vibration for Flexible Pipes

Ching Sheng Ooi[1]*, Meng Hee Lim[1], Kee Quen Lee[2], Hooi Siang Kang[3,4] and Mohd Salman Leong[1]

[1]Institute of Noise and Vibration, Universiti Teknologi Malaysia, 54100 Kuala Lumpur, Malaysia
[2]Intelligent Dynamic and System I-kohza, Malaysian-Japan International of Technology, Universiti Teknologi Malaysia, 54100 Kuala Lumpur, Malaysia
[3]School of Mechanical Engineering, Faculty of Engineering, Universiti Teknologi Malaysia, 81310 Johor Bahru, Malaysia
[4]Marine Technology Center, Universiti Teknologi Malaysia, 81310 Johor Bahru, Johor, Malaysia

ABSTRACT

Previous studies have indicated that the pipe-surface-mounted helical strakes effectively reduce vortex-induced vibration (VIV) under a uniform flow application, particularly during the lock-in region. Since VIV experiments are time-consuming, observation is generated with an interval helical strakes parameter in pitch and height to lessen tedious procedures and repetitive post-processing analyses. The aforementioned result subset is insufficient for helical strakes design optimisation because the trade-off between the helical strakes dimension, lock-in region and flow velocity are non-trivial. Thus, a parametric model based on an improved recursive least squares (RLS) parameter estimation technique is proposed to define the statistical relationship between input, or strakes and pipe dimension, and output, or VIV amplitude ratio. As results suggested, revised RLS estimated VIV model demonstrated an optimal prediction with the highest coefficient of determination and lowest Integral Absolute Error. The feasibility of VIV parametric model was validated by embed into Genetic Algorithm (GA) as the fitness function to acquire a desirable helical strakes dimension with minimum VIV amplitude. The rapid generation of optimal helical strakes dimension which returned the highest VIV suppression implied a superior simulation method compared to the experimental outcome.

Keywords: Genetic algorithm, helical strakes, recursive least squares, vortex-induced vibration

ARTICLE INFO

Article history:
Received: 04 October 2019
Accepted: 07 February 2020
Published: 15 April 2020

E-mail addresses:
chingshengooi@gmail.com (Ching Sheng Ooi)
limmenghee@gmail.com (Meng Hee Lim)
lkquen@utm.my (Kee Quen Lee)
kanghs@utm.my (Hooi Siang Kang)
salman.leong@gmail.com (Mohd Salman Leong)
* Corresponding author

ISSN: 0128-7680
e-ISSN: 2231-8526

INTRODUCTION

Vortex-induced vibration (VIV) is defined as the oscillation of a structure when subjected to the influence of fluids in motion. When synchronization between shedding vortex and structural natural frequency takes place, a unique occurrence, the lock-in region, results from VIV magnitude amplification (Chizfahm et al., 2018). This undesirable event generates excessive hydrodynamic, lift and drag force which leads to material property degradation. Consequently, equipment and accessories with a relatively high aspect ratio and low mass ratio, such as risers, airplane wings, and turbine blades, are prone to fatigue after exposure to VIV over a certain period. However, the aforementioned parts are critical components in the system as a whole; thus, undermining VIV development would limit basic component functionality, system efficiency, and contribute to disastrous incident.

In recent years, numerous research efforts have dedicated themselves to understanding the causes of VIV so as to minimize the effects on structural integrity. For example, a two degree higher-order nonlinear oscillator model was developed, aiming to perform VIV forecast for cylinders with respect to mass ratio and damping ratio (Kang et al., 2018). The model and parameter sensitivity were built on the fundamental Van der Pol equation, which had been validated with experimental outcomes. A virtual damping–spring (VCK) based variable added mass system yield mean damped natural frequency approximately matched oscillating frequency while the phase between force and displacement levelled with VIV lock-in range resonance in perpendicular direction (Garcia & Bernitsas, 2018). The VCK-based method is practical to find suitable mass increments for VIV suppression purposes.

On the other hand, a reduced order model deduced from a high-fidelity analysis of sectional pipe is employed for in-line and cross-flow oscillation measures (Stabile et al., 2018). Performance of the reduced order model is subjected to system-parameter identification to obtain full scale indication. Based on the Scale-Adaptive Simulation $(k-\omega\, SST-SAS)$ model, twisted design has been found capable of diverting hydrodynamic force with respect to cylinder length direction when compared to conventional square shapes (Wu et al., 2018). A novel image processing EFD/SVM has been proposed to detect and identify segments of VIV wake-patterns in a non-destructive manner for effective classification outcomes (Lin, 2018). By combining time domain and filtered VIV frequency responses, an improved semi-empirical predictor is established to track wave profiles regardless of steady uniform or turbulent flow (Ulveseter et al., 2018).

A new VIV wake oscillator provides appropriate prediction by considering the Reynolds number, lock-in regions and peak-amplitude formulae as estimation functions (Gao et al., 2018). Parameter identification techniques have been applied to gain VIV amplitude, frequency, and phase lag from time domain vortex induced hydrodynamic force using computational fluid dynamics (CFD) simulation (Pigazzini et al., 2018). In order

to eliminate premature convergence in VIV modal space prediction, a non-iterative root search is selected to solve hydrodynamic force and dynamic response equations together without power-balance (Lu et al., 2018). GA has been adopted in Facchinetti variable optimization to allow greater efficiency in flow induced vibration energy harvesting (Ashok et al., 2018). For aeroelastic force modelling, positive curvature in circular structures has proven effective in cross-wind oscillation damping (Lupi et al., 2018). A hybrid Euler-Van der Pol equation is coupled with the Newmark-beta method to explain VIV response of marine risers in three-dimensional space, including in-line, cross-flow, and structural dynamics (Komachi et al., 2018). The simulation is able to develop conclusions regarding stress-fatigue proportionality.

A VIV-related literature review demonstrates that extensive knowledge has been acquired over years of thoughtful investigation, ranging from experimental studies to numerical simulation modelling. The adopted countermeasure approaches involving product design modification in conjunction with suppression tools and excessive VIV value monitoring have proven to be useful. Nonetheless, modelling techniques require an understanding of sophisticated mathematical equations and posteriori-based assumptions. In addition, it is laborious to conduct exhaustive experiments in a repetitive manner. Due to VIV turbulent characteristics and various manipulating variables, obtaining a practical, universal solution is a tedious process.

As a result, the objective of this case study was to demonstrate a straightforward system identification methodology to identify VIV mathematical relationship. The simulation deployed VIV amplitude data collection when helical strakes acted as suppression tool for flexible risers (Quen et al., 2014). A feasible system identification technique was implemented to estimate unknown parameters with a target of fitting VIV curves given the strakes dimension input and flow velocity range. The particular method of improved RLS was selected due to its accuracy and iterative estimation update nature. The performance of the VIV model was validated using GA by means of a fitness function searching for optimal strakes dimension, which generated minimal VIV response. Section 2 describes the methodology of RLS in detail, following by experiment setup. Section 3 tabulates hindsight on simulation findings.

MATERIALS AND METHODS

The case study focused on VIV generated under uniform flow application, as experimented in (Quen et al., 2014). The controlled data measurement procedure is explained, followed by the presentation of novel parameter estimation technique and Matlab software simulation design.

Experimental Setup

A poly vinyl chloride (PVC) cylinder was operated as the riser model with settings as detailed in Table 1. The highly flexible cylinder was designed to move freely in an axial direction at one end and in restricted torsion effect with universal joints at both ends. Detailed riser configurations can be found in Sanaati and Kato (2013).

Table 1
Helical strakes and risers' parameters

Outer diameter (D)	18 *mm*
Inner diameter (d)	13 *mm*
Length (L)	2.92 *m*
Pre-tension (T)	147 *N*
Bending stiffness (El)	9.0 Nm^2
Spring stiffness (k_s)	6.5 *N/m*
Cylinder axial stiffness (*EA/L*)	100 *N/mm*
Cylinder air weight	1.64 *N/m*
Total weight including internal water (*m*)	2.97 *N/m*
Mass ratio	1.17
Damping ratio (*z*)	0.028
Applied strakes' height (*h*)	0.05D, 0.1D, 0.15D
Applied strakes' pitch (*p*)	5D, 10D, 15D
Number of helix	3-start helical
Flow speed (*U*)	0.1-1.0 *m/s*
Subcritical Reynolds number range (*Re*)	1380-13,800
Natural frequency (f_n)	2.92, 2.82, 2.82, 2.86, 2.85, 2.78

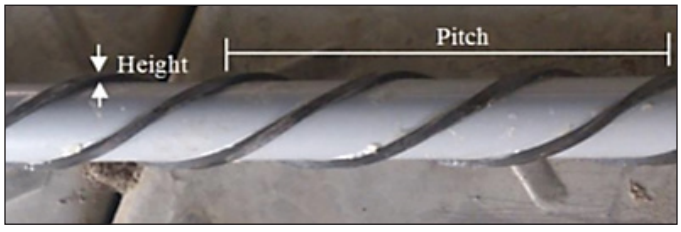

Figure 1. Schematic diagram of cylinder pipe with three-start helical strakes

The cylinder specimens were soaked at a 0.35 m depth from the water surface level in a basin of 100 *m* × 7.8 *m* × 4.35 *m* and were towed to create a uniform flow speed, *U*. To initiate a subcritical Reynolds number, *U* was regulated between 0.1 and 1.0 *m/s*, with a step increment of 0.03 *m/s*. As displayed in Figure 1, The strakes' dimension was increased gradually from 0.05 to 0.15 times the cylinder diameter in height and 5 to 15 times the cylinder diameter for pitch length, respectively. Hence, 25-cylinder towing speed

steps were repeated for six unique strakes combinations ($N = 6$). The strakes' dimension range is defined based on laminar boundary layer thickness, as measured by Pohlausen's approximation. For every strakes setup, the vibration response was recorded using a charge-coupled device (CCD) camera installed at the centre of the cylinder before being analysed by a motion-tracking software. Additionally, thorough experiment information can be obtained in Sanaati's description (Sanaati, 2012).

Vibration amplitude for strakes application was examined in contrast to the bare cylinder baseline amplitude ratio. The comparison is expressed using amplitude ratio (*AR*), and reduced velocity (V_r). The *AR* is defined as the normalisation of the standard deviation of time series vibration amplitude reading with respect to the outer diameter of the cylinder ($AR = A_\sigma/D$). The reduced velocity, $V_r = U/f_nD$, indicates the scaling of uniform cylinder towing speed, U, as a function of its natural frequency and outer diameter. Based on 25 regular step intervals of U, the V_r values are pre-set within a range of 1.909 and 17.755. Dimensionless *AR* and V_r indications are chosen as the variables for y-axis and x-axis respectively. Therefore, the *AR* value represents induced vibration weightage to the corresponding reduced velocity. The presented amplitude ratio versus reduced velocity measurement is an appropriate VIV reduction instrument when cylinder diameter variation is of concern.

System Identification Technique: Recursive Least Square Parameter Estimation

The least squares (LS) technique was developed by C. F. Gauss initially to estimate planet orbital motion (Young, 2011). In present, LS has evolved to estimate a fitting curve through measurement points. The fitting curve is described as a line which contains a minimal sum squared error when compared to available measurement points. For example, given the *nth* order difference equation, as below:

$$y_{0k} = a_1 x_{k1} + a_2 x_{k2} + \cdots + a_n x_{kn} \quad (1)$$

where output y_{0k} is the summation of n number of parameter α multiply input data x for *kth* data observation. Reorganizing Equation 1 into a stacked equation for linearity purpose provides:

$$y_{0k} = [x_{k1}\ x_{k2}\ \cdots\ x_{kn}\ ][\alpha_1\ \alpha_2\ \ldots\ \alpha_n\ ] = \varphi_k^T\theta \quad (2)$$

For *kth* observation, $\varphi_k \epsilon R^n$ is denoted as the regressor vector with n input data while θ is regarded as parameter vector. Both regressor vector and parameter vector comprises of n real number elements. If the data observation is repeated for N iteration time, the Equation 2 can be summarised in Equation 3 for $k = 1,2, \ldots, N-1,N$:

$$\begin{bmatrix} y_{0_1} \\ y_{0_2} \\ \vdots \\ y_{0_N} \end{bmatrix} = \begin{bmatrix} x_{11} & x_{12} & \cdots & x_{1n} \\ x_{21} & x_{22} & \cdots & x_{2n} \\ \vdots & \vdots & \ddots & \vdots \\ x_{N1} & x_{N2} & \cdots & x_{Nn} \end{bmatrix} \begin{bmatrix} \alpha_1 \\ \alpha_2 \\ \vdots \\ \alpha_n \end{bmatrix}$$

$$Y_0 \approx \Phi\theta \tag{3}$$

where $Y_0 \epsilon R^N$ represents a vector consists of N stacked real number output signals, y_{0k} while input data matrix, $\Phi \epsilon R^{N \times n}$ is the combination of N row of regressor vector, φ_k. However, due to uncertainties such as measurement errors and inconsistency, output generally possesses noise sequence, e_k. Equation 3 becomes $Y = \Phi\theta + e$, where Y is the summation of Y_0 and stacked error vector, e. A cost function, V with argument θ is then introduced to minimise curve fitting error (Equation 4):

$$V(\theta) = \frac{1}{2}\sum_{k=1}^{N} \varepsilon_k^2 = \frac{1}{2}\varepsilon^T\varepsilon = \frac{1}{2}\|\varepsilon\|^2 \tag{4}$$

where ε is the residual of model output. Thus, LS optimization was achieved via sum squared error minimisation, as presented in Söderström and Stoica (2002).

$$\begin{aligned} arg\min_{\theta} V(\theta) &= \frac{1}{2}(Y - \Phi\theta)^T(Y - \Phi\theta) \\ &= \frac{1}{2}(Y^TY - Y^T\Phi\theta - \theta^T\Phi^TY + \theta^T\Phi^T\Phi\theta) \end{aligned} \tag{5}$$

Minimum error value is obtained by setting a partial derivative of Equation 5 to zero:

$$\frac{\partial V(\theta)}{\partial\theta} = -\Phi^TY + \Phi^T\Phi\theta \tag{6}$$

Then, rearranging input and output in Equation 6 provides the LS estimated parameter solution, $\hat{\theta}$:

$$\hat{\theta} = (\Phi^T\Phi)^{-1}\Phi^TY \tag{7}$$

Noting that $(\Phi^T\Phi)^{-1}$ is known as covariance matrix P. Equation 7 can be modified recursively over N observations, if elements for $k = 1, 2, \ldots, N-1, N$ observation are known.

$$P_k^{-1} = P_{k-1}^{-1} + \varphi_k\varphi_k^T \tag{8}$$

$$\hat{\theta}_{k-1} = P_{k-1}\sum_{i=1}^{k-1}\varphi_i y_i$$

$$\sum_{i=1}^{k-1}\varphi_i y_i = P_{k-1}^{-1}\hat{\theta}_{k-1}$$

$$\hat{\theta}_k = P_k\left(P_{k-1}^{-1}\hat{\theta}_{k-1} + \varphi_k y_k\right) \quad (9)$$

By updating Equation 8 into Equation 9, the one-step ahead prediction using RLS is obtained:

$$\begin{aligned}\hat{\theta}_k &= P_k\left[\left(P_k^{-1} + \varphi_k\varphi_k^T\right)\hat{\theta}_{k-1} + \varphi_k y_k\right] \\ &= \hat{\theta}_{k-1} + P_k\varphi_k\left(y_k - \varphi_k^T\hat{\theta}_{k-1}\right)\end{aligned} \quad (10)$$

where $\left(y_k - \varphi_k^T\hat{\theta}_{k-1}\right)$ is denoted as one-step ahead prediction error and $P_k\varphi_k$ is the correction gain updated from gain vector L_k denoted by expansion of Equation 8 with matrix inversion lemma (Hostetter, 1987):

$$L_k = P_{k-1}\varphi_k\left(1 + \varphi_k^T P_{k-1}\varphi_k\right)^{-1} \quad (11)$$

$$P_k = P_{k-1} - L_k\varphi_k^T P_{k-1} \quad (12)$$

The notable difference between LS and RLS is that LS consider stacked regressor vector and targeted output simultaneously, as explained in Equation 7, whilst RLS perform parameter estimation fine-tuning over *N* iterations. The recursive update algorithm offers an advantage over standard LS by using less bulky dataset and better convergence, particularly with complex dataset problems accompanied by limited data sampling *N*. By means of a less bulky dataset, RLS only require an estimated parameter vector from the previous iteration and input and output data from the current observation to perform a parameter estimation and correction gain update (refer to Equation 10, 11 and 12). However, the iterative update algorithm requires additional computational effort as compared to the LS estimation in Equation 7 (Wang & Ding, 2013).

Recent RLS development comprises measuring the dynamic behaviour of excavators with rotational inertia (Oh & Seo, 2018), motion synchronisation controller fine-tuning for gimbal systems (Lee & Jung, 2018), battery pack insulation fault detection for electric vehicles (EVs) (Tian et al., 2018), time-dependent Surface Processes and Acoustic Communication Experiment (SPACE08) underwater communication channel tracking

with a graphical model (Yellepeddi & Preisig, 2018), and estimation of disturbance signal embedded in active vibration control (AVC) feedback mechanisms for a closed-loop damping system model (Oveisi et al., 2018).

Recursive Least Square Parameter Estimation Simulation Integrated Development Environment

The VIV experiment dataset is subject to LS and RLS simulations using *Matlab* software R2019a. For every step of V_r, parameter estimation techniques generate $\hat{\theta}$ by observing AR experiment results of six unique strake dimensions ($N = 6$) as output and n matching strakes dimension input. In other words, LS and RLS estimate n weighting coefficients corresponding to every V_r with the target of simulate actual AR value with minimal squared error. The estimated parameter vector is designed to contain two elements in accordance with strakes' height and pitch dimensions. When the $\hat{\theta}$ desired is identified, only the strake dimension is needed to simulate AR as predicted output, $\hat{y}$.

It is worth mentioning that estimated parameter elements are assigned as zero during standard LS and RLS initialisation to avoid bias. Alternatively, for improved RLS, the LS estimated parameter vector is set up as the initial estimated parameter instead of zero vector, $\hat{\theta}_{RLS,N=1} = \hat{\theta}_{LS}$. The argument is that the additional parameter re-evaluation stage could provide faster convergence, especially for current VIV dataset with limited amount of observation data N. Standard estimation performance indicators such as coefficient of determination R_T^2 and integral absolute error (*IAE*) are measured to quantify the output variation between estimation model simulation and VIV experiment dataset.

Lastly, the most probable AR estimation model is substituted as the GA fitness function in *Matlab* software. The GA platform performs a heuristic search for the minimum of a given function. For VIV case studies specifically, GA is responsible for discovering optimal strakes input dimensions, which yield minimal fitness function output AR. The minimal fitness function output criterion includes both the minimum global maxima AR value over V_r range, and minimum average AR value.

The desirable estimated parameter is updated into Equation 3 prior the simulation as a fitness function for *Matlab* syntax *ga*. The input variables for *ga* fitness function are the strakes' pitch and height. All unique strakes' input combinations within the search boundary are considered as potential solutions. A heuristically defined strakes dimension which simulate unprecedented minimum global maxima and average AR is selected as the optimal strakes candidate and benchmark for the next GA iteration. The GA iterative process is terminated when the following condition is met: either there has been no improvement over a predetermined period cycle or the target value has been achieved. The iterative simulation process overview is exhibited in Figure 2. The simulation results and discussion are presented in the next section.

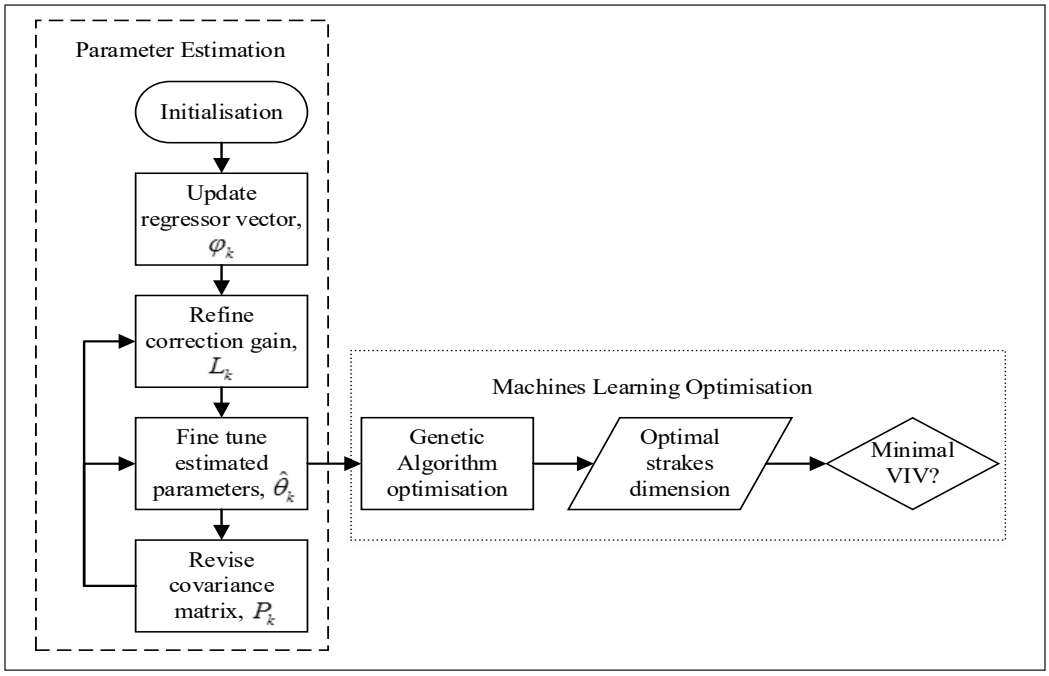

Figure 2. RLS parameter estimation iterative process for Machine Learning Optimisation

RESULTS AND DISCUSSION

First, improved RLS, standard RLS, and LS simulated outputs are compared to actual experiment results with identical strakes' dimensions by employing standard estimation measures: R_T^2 and *IAE*. $\hat{y}$ is the simulated output and *y* is the actual output. The next step includes embedding the estimation model with the highest accuracy as GA fitness function to identify optimal strakes' dimensions with minimal AR response.

Table 2
Model efficacy for parameter estimation techniques

Strakes dimension			$R_T^2 = \frac{\sum(\hat{y}-y)^2}{\sum(y-\bar{y})^2}$		$IAE = \frac{\sum(\hat{y}-y)}{N}$	
Setting	Pitch	Height	LS and RLS	Improved RLS	LS and RLS	Improved RLS
1	0	0	80.8%	40.3%	0.063	0.111
2	5*D	0.1*D	86.4%	88.1%	0.031	0.026
3	10*D	0.05*D	85.9%	97.4%	0.034	0.014
4	10*D	0.1*D	19.1%	73.1%	0.038	0.021
5	15*D	0.1*D	-380.7%	-139.0%	0.033	0.027
6	10*D	0.15*D	82.3%	95.0%	0.021	0.013

Table 2 depicts the efficacy results using three parameter estimation techniques: LS, RLS and improved RLS. The closer the model performance is to 100 percent R_T^2 and zero *IAE*, the more representative the estimated parameter is in reflecting actual output. Overall, for six strakes' dimension settings, apart from bare cylinder, the improved RLS method provides better R_T^2 and *IAE* indication. This observation is likely caused by the RLS algorithm trade-off of bare cylinder AR tracking accuracy for cylinder with additional strakes. Although LS and RLS sufficiently simulated AR with a majority R_T^2 over 80% and *IAE* lower than 0.04, an improved RLS is still capable of enhancing the efficacy by minor fine-tuning of the estimated parameter.

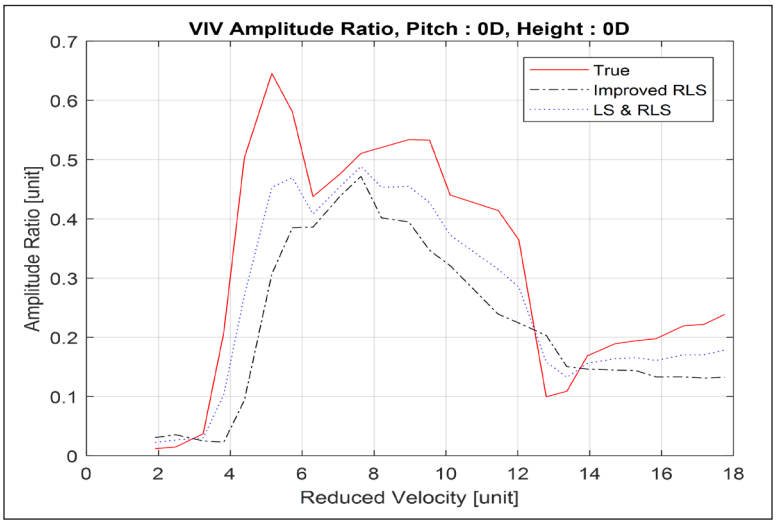

Figure 3. AR versus V_r for setting: 1

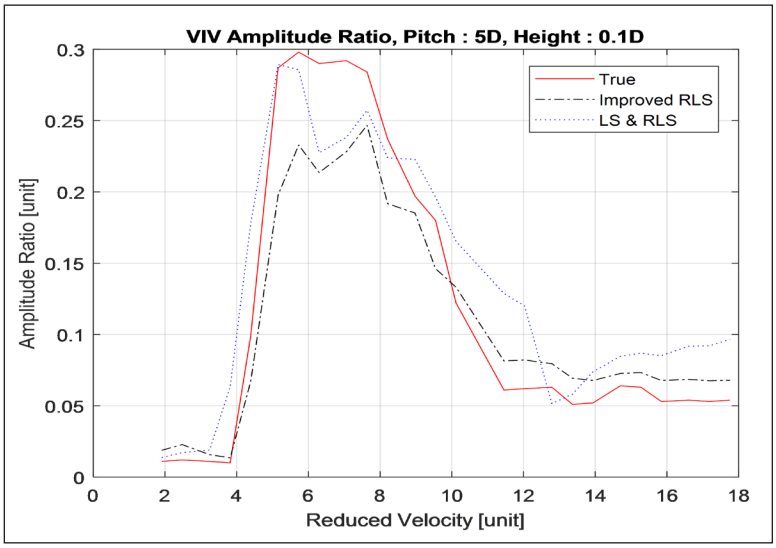

Figure 4. AR versus V_r for setting: 2

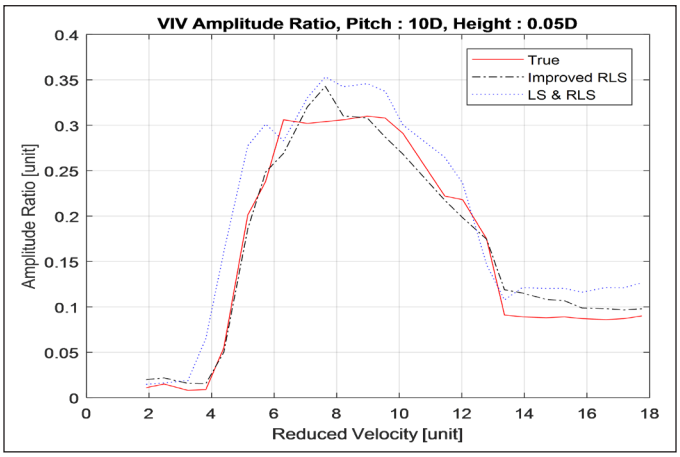

Figure 5. AR versus V_r for setting: 3

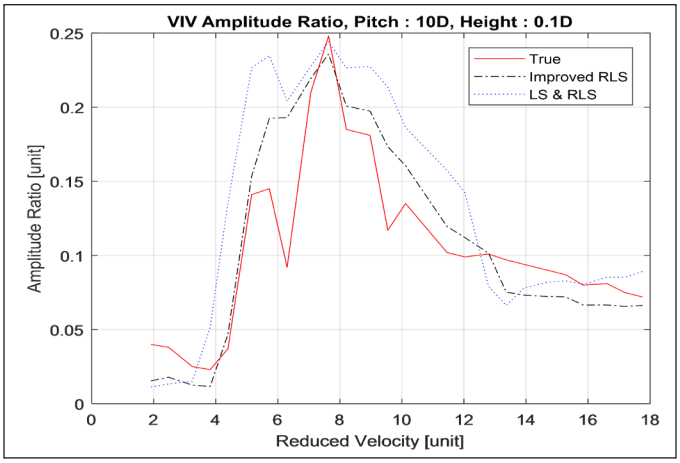

Figure 6. AR versus V_r for setting: 4

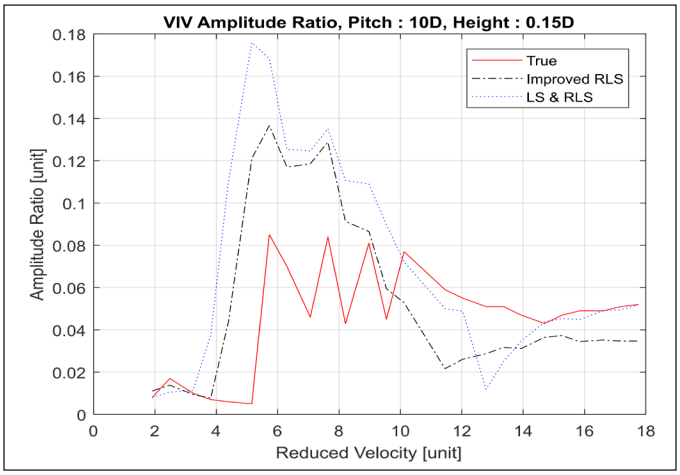

Figure 7. AR versus V_r for setting: 5

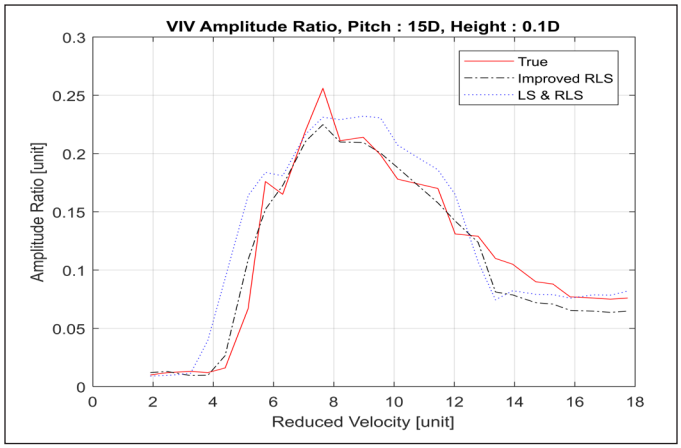

Figure 8. AR versus V_r for setting: 6

Figure 3 to 8 exhibit the VIV parameter model simulation outcomes against actual experimental result for 6 different strakes dimension setting. Preliminary inspection revealed that the majority of the tracking errors occured near lock-in regions since AR changes were more rapid, with steep slopes and spikes. The prediction error is likely due to influence from external factors and insufficient data sampling. As a result, all related models suffer the most errors whilst tracking strakes dimension with 10 times diameter in pitch and 0.15 times diameter in height, the fifth strakes' setting. However, compared to classic LS and RLS, improved RLS is still capable of simulating AR with resemble lock-in patterns when strakes material is present. The visible similarity between improved RLS simulated output and actual AR around the lock-in regions is of concern in VIV suppression. Hence, it can be concluded that the improved RLS algorithm produced the most probable estimated parameters for the given dataset.

The advantage of improved RLS in numerical analysis and visualisation is further supported in Figure 9 with the trace of covariance matrix, P over six observations in a semilog scale. It can be noticed that P for the improved RLS method gradually converged from 2^{10} to 8.381 at the end of the simulation, which is equivalent to the value acquired by standard the LS and RLS. Even though the LS method experienced convergence at the end of the simulation, the improved RLS identified room for improvement through adaptive correction gains and by using $\hat{\theta}_{LS}$ as an initial estimated parameter.

To perform strakes' dimension optimisation, the search space is set to cover solely the given dataset range since AR behaviour is uncertain beyond range boundary. Additionally, after conducting AR observations, it is believed that the minimal AR value is likely to vary between the fifth and sixth settings. With the improved RLS estimation model as fitness function, the GA simulation discover the optimal strakes' dimension as 14.02 times D and 0.16 times D for pitch and height, respectively. This has been validated by comparing the

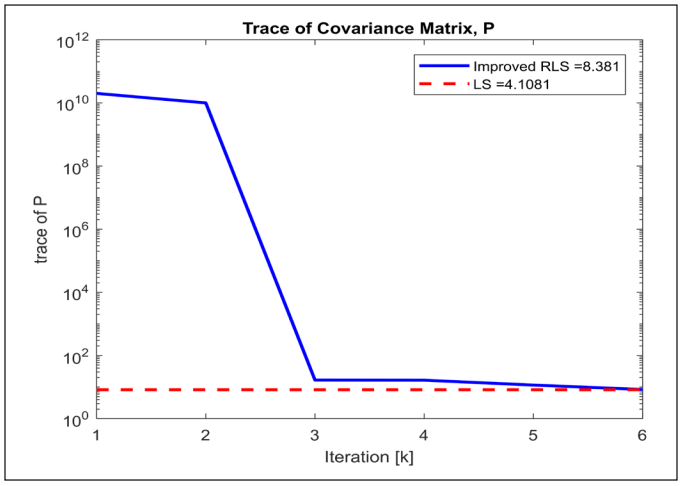

Figure 9. Trace of Covariance Matrix, P

AR simulated by GA-generated optimal strakes input and the fifth strakes setting using the improved RLS model. GA data evaluation in Table 3 shows that global maxima and average AR revealed with GA-simulated optimal strakes are considerably lower than the fifth setting. Figure 10 further illustrates that GA-simulated optimal strakes provide better VIV suppression over fifth strakes setting, particularly around the lock-in region (V_r ranging from 4 to 10). GA-simulated optimal strakes were deemed to be more superior since less strakes material is required to perform optimum suppression effects. This outcome evidenced the feasibility of performing system identification of VIV responses to obtain an optimal dimension of suppression tools, with a representable dataset and estimated parameter.

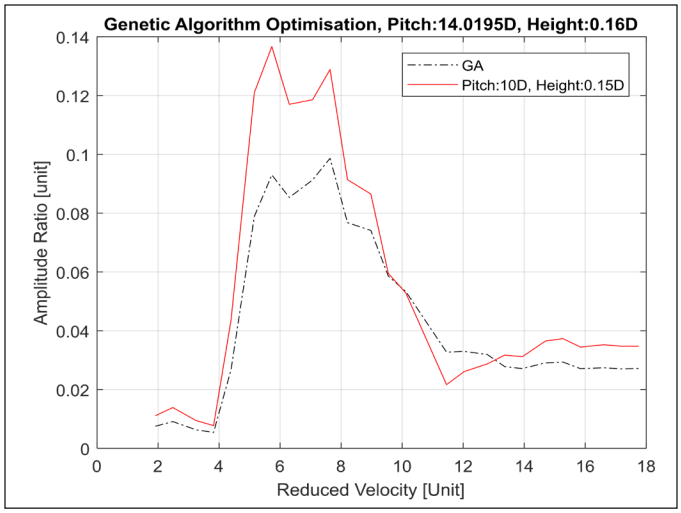

Figure 10. AR for GA-simulated optimal strakes dimension and setting: 5

Table 3
GA optimisation evaluation

Setting	Pitch	Height	Global Maxima AR	Average AR
GA	14.02*D	0.16*D	0.10	0.043
5	15*D	0.1*D	0.14	0.054

CONCLUSIONS

The present investigation involves the system identification of helical strakes suppressed VIV for PVC pipes. With respect to the provided dataset, the VIV response simulated by a proposed improved RLS technique stipulates a satisfactory outcome compare to the actual values. Standard parameter estimation methods benchmarking suggested that the improved RLS model is a fast and accurate option to assist an experimental approach in VIV monitoring. Not only can minimal VIV response be obtained by indicating optimal strakes dimensions, an improved RLS model embedded GA also helped to eliminate trial-and-error processes when conducting VIV experiments. Nonetheless, it is inevitable that the model accuracy plunges as the VIV is suppressed due to turbulent lock-in region behaviour and unpredictable changes. Improvement can be achieved with an optimal strakes range extension which requires further experimental initiative.

ACKNOWLEDGMENTS

This work was supported in part by the Institute of Noise and Vibration UTM through the Higher Institution Centre of Excellence (HICoE) under Grant R.K130000.7809.4J226, Grant R.K130000.7809.4J227, and Grant R.K130000.7809.4J228, and in part by the UTM Research University under Grant Q.K130000.2543.11H36.

REFERENCES

Ashok, P., Chandra, C. J., Neeraj, P., & Santhosh, B. (2018). Parametric study and optimization of a Piezoelectric energy harvester from flow induced vibration. *IOP Conference Series: Materials Science and Engineering, 310*, 1-10.

Chizfahm, A., Yazdi, E. A., & Eghtesad, M. (2018). Dynamic modeling of vortex induced vibration wind turbines. *Renewable Energy, 121*, 632-643.

Gao, X. F., Xie, W. D., Xu, W. H., Bai, Y. C., & Zhu, H. T. (2018). A novel wake oscillator model for vortex-induced vibrations prediction of a cylinder considering the influence of Reynolds number. *China Ocean Engineering, 32*(2), 132-143.

Garcia, E. M. H., & Bernitsas, M. M. (2018). Effect of damping on variable added mass and lift of circular cylinders in vortex-induced vibrations. *Journal of Fluids and Structures, 80*, 451-472.

Hostetter, G. H. (1987). Chapter 13 – Recursive estimation. In D. F. Elliott (Ed.), *Handbook of digital signal processing* (pp. 899-940). New York, NY: Academic Press.

Kang, Z., Zhang, C., & Chang, R. (2018). A higher-order nonlinear oscillator model for coupled cross-flow and in-line VIV of a circular cylinder. *Ships and Offshore Structures, 13*(5), 488-503.

Komachi, Y., Mazaheri, S., & Tabesgpour, M. R. (2018). Wake and structure model for simulation of cross-flow/in-line vortex induced vibration of marine risers. *Journal of Vibroengineering, 20*(1), 152-164.

Lee, S. D., & Jung, S. (2018). An adaptive control technique for motion synchronization by on-line estimation of a recursive least square method. *International Journal of Control, Automation and Systems, 16*(3), 1103-1111.

Lin, T. K. (2018). An edge-feature-description-based scheme combined with support vector machine for the detection of vortex-induced vibration. *International Journal of Innovative Computing, Information and Control, 14*(3), 833-845.

Lu, Z., Fu, S., Zhang, M., Ren, H., & Song, L. (2018). A modal space based direct method for vortex-induced vibration prediction of flexible risers. *Ocean Engineering, 152*, 191-202.

Lupi, F., Niemann, H. J., & Höffer, R. (2018). Aerodynamic damping model in vortex-induced vibrations for wind engineering applications. *Journal of Wind Engineering and Industrial Aerodynamics, 174*, 281-295.

Oh, K. S., & Seo, J. H. (2018). Inertia parameter estimation of an excavator with adaptive update rule using performance analysis of kalman filter. *International Journal of Control, Automation and Systems, 16*(3), 1226-1238.

Oveisi, A., Hosseini-Pishrobat, M., Nestorović, T., & Keighobadi, J. (2018). Observer-based repetitive model predictive control in active vibration suppression. *Structural Control and Health Monitoring, 25*(5), 1-23.

Pigazzini, R., Contento, G., Martini, S., Puzzer, T., Morgut, M., & Mola, A. (2018). VIV analysis of a single elastically-mounted 2D cylinder: Parameter Identification of a single-degree-of-freedom multi-frequency model. *Journal of Fluids and Structures*, *78*, 299-313.

Quen, L. K., Abu, A., Kato, N., Muhamad, P., Sahekhaini, A., & Abdullah, H. (2014). Investigation on the effectiveness of helical strakes in suppressing VIV of flexible riser. *Applied Ocean Research, 44*, 82-91.

Sanaati, B. (2012). *An experimental study on the VIV hydrodynamics of pre-tensioned flexible cylinders with single and multiple configurations* (PhD thesis). Osaka University, Japan.

Sanaati, B., & Kato, N. J. (2013). Vortex-induced vibration (VIV) dynamics of a tensioned flexible cylinder subjected to uniform cross-flow. *Journal of Marine Science and Technology, 18*(2), 247-261.

Söderström, T., & Stoica, P. (2002). Instrumental variable methods for system identification. *Circuits Systems and Signal Process, 21*, 1-9.

Stabile, G., Matthies, H. G., & Borri, C. (2018). A novel reduced order model for vortex induced vibrations of long flexible cylinders. *Ocean Engineering, 156*, 191-207.

Tian, J., Wang, Y., Yang, D., Zhang, X., & Chen, Z. (2018). A real-time insulation detection method for battery packs used in electric vehicles. *Journal of Power Sources, 385*, 1-9.

Ulveseter, J. V., Thorsen, M. J., Sævik, S., & Larsen, C. M. (2018). Time domain simulation of riser VIV in current and irregular waves. *Marine Structures, 60*, 241-260.

Wang, S., & Ding, R. (2013). Three-stage recursive least squares parameter estimation for controlled autoregressive autoregressive systems. *Applied Mathematical Modelling, 37*(12-13), 7489-7497.

Wu, C. H., Ma, S., Kang, C. W., Lim, T. B. A., Jaiman, R. K., Weymouth, G., & Tutty, O. (2018). Suppression of vortex-induced vibration of a square cylinder via continuous twisting at moderate Reynolds numbers. *Journal of Wind Engineering and Industrial Aerodynamics, 177*, 136-154.

Yellepeddi, A., & Preisig, J. C. (2018). Efficient system tracking with decomposition graphic-structured inputs and application to adaptive equalization with cyclostationary inputs. *IEEE Transaction on Signal Processing, 66*(10), 2645-2658.

Young, P. C. (2011) Recursive least squares estimation. In C. P. Young (Ed.), *Recursive estimation and time-series analysis* (pp. 29-46). Heidelberg, Germany: Springer.